AIAA JOURNAL
Vol. 33, No. 8, August 1995

Lower-Upper Scheme for Chemically Reacting Flow with Finite Rate Chemistry

Yiguang Ju*
Tohoku University, Sendai 980-77, Japan

A fourth-order shock-capturing scheme has been developed for steady-state and time-accurate simulation of chemically reacting flows with finite rate chemical kinetics. A diagonal algorithm and a local implicit technique are presented to remove the stiffness of chemical reaction and to achieve high computation efficiency. A fully implicit code is obtained by combining the present algorithm with the lower-upper scheme. The validity of this code is demonstrated by calculating the unsteady shocks in an inviscid supersonic duct and by comparing the results with the previous calculation. Then the code is used to calculate the ignition of a premixed hydrogen/air reacting flow in a ramped duct and nonpremixed hydrogen/air streams as well as nonpremixed methane/air streams in a supersonic mixing layer. The efficiency and robustness of the present scheme are shown through these numerical simulations.

Introduction

THE development of supersonic vehicles requires high-resolution numerical schemes to predict accurately the phenomenon of ignition and combustion in scramjet engines. Additionally, since neither adiabatic equilibrium nor global chemistry are capable of accurately investigating crucial design questions, detailed finite rate chemical kinetics should be included into these schemes.

Recently, based on the total variation diminishing (TVD) condition, several kinds of TVD schemes have been constructed. These schemes[1–3] are successfully and widely used for capturing shock waves. However, the preceding schemes only have at most second- or third-order accuracy results, except for the location near contact discontinuity. To improve the numerical resolution, a fourth-order compact MUSCL TVD scheme has been presented by Yamamoto and Daiguji.[4] Their results showed that its resolution is higher than that of the existing TVD scheme. However, this scheme has not been developed to consider the real gas effect and chemical kinetics.

The use of detailed chemical kinetics results in the stiffness problem from the presence of chemical source terms. Currently, there are three kinds of methods to eliminate this stiffness. The first one is to uncouple the species equations from the fluid dynamic equation and solve them sequentially.[5,6] The second one is to use a point-implicit numerical scheme where species equations are solved by inverting the block matrices at each grid point while convection terms are treated explicitly.[7,8] The third method solves both the species equations and the convective fluid dynamic equations in a coupled fully implicit form.[9,10] The first method has the advantage that it can be easily implemented. However, this uncoupled method encountered the problem of maintaining numerical stability. The second method eliminates the stiffness, but stability is strictly limited by the Courant–Friedrichs–Lewy (CFL) condition. The third method has successfully removed the CFL condition but is very time consuming. Shuen and Yoon[11] and Yu et al.[12] then developed lower-upper (LU) scheme to improve the efficiency of the implicit solver of convective terms. However, the inversion of block matrices of source terms at each grid point is still needed. In addition, instead of solving the conservation equations of n species (total number of species), they solved the total mass conservation equation and $n-1$ species equations. This method has the advantage that the existing Navier–Stokes equation solution algorithm can be used directly. However, since all of the computation errors will be added to the nth species, the mass fraction of nth species may not be correctly predicted in complex reacting flows.

To overcome these two disadvantages, computational expense and conservation of nth species, Eberhadt and Imlay[13] presented a diagonal algorithm with coupled n species equations for steady-state problems. Their algorithm dramatically improved the computational efficiency and first showed us the possibility of using a diagonal scheme for steady-state reacting flow. However, recent study has shown that, although their algorithm is stable, in some cases, such as ignition, it does not converge to the physical solution. The reason may be that their definition of characteristics reaction time does not reflect the physical chemical reaction time.

In this paper, first the fourth-order MUSCL scheme[4] in conjunction with Steger–Warming flux vector splitting is developed for the simulation of unsteady multidimensional chemical reacting flow in a generalized coordinate. Species equations are solved in a fully coupled fashion. Then, based on the analysis of chemical kinetics, a diagonal algorithm and a local implicit technique are given, respectively, for simulating steady-state and time-accurate chemically reacting flows with finite rate chemistry. A fully implicit scheme is obtained by combining these algorithms with the LU-SGS scheme. Finally, the present scheme is used to calculate the shocks of an unsteady supersonic duct flow. This is followed by the computation of ignitions of a premixed hydrogen/air mixture in a ramped duct and nonpremixed hydrogen/air and methane/air streams in a supersonic mixing layer. Comparisons of the diagonal algorithm and the local implicit algorithm with point implicit scheme are made.

Governing Equations

The nondimensional Navier–Stokes equations in generalized curvilinear coordinate (ξ, η, ζ) for a time-dependent, multidimensional, chemically reacting flow with n species and finite rate chemistry can be written as

$$\frac{\partial \hat{U}}{\partial t}+\frac{\partial \hat{E}}{\partial \xi}+\frac{\partial \hat{F}}{\partial \eta}+\frac{\partial \hat{G}}{\partial \zeta}=\frac{\partial \hat{E}_v}{\partial \xi}+\frac{\partial \hat{F}_v}{\partial \eta}+\frac{\partial \hat{G}_v}{\partial \zeta}+\hat{S} \quad (1)$$

where $\hat{U}$ is the vector of conservation variables; $\hat{E}$, $\hat{F}$, and $\hat{G}$ are, respectively, the vectors of convective fluxes; $\hat{E}_v$, $\hat{F}_v$, and $\hat{G}_v$ are their corresponding viscous fluxes; and $\hat{S}$ is a vector of the source term of chemical reaction. For illustration, vectors $\hat{U}$, $\hat{E}$, $\hat{E}_v$, and $\hat{S}$ are written here. Detailed description of the other vectors was given in Ref. 14:

Received May 17, 1994; revision received Jan. 31, 1995; accepted for publication Jan. 31, 1995. Copyright © 1995 by the American Institute of Aeronautics and Astronautics, Inc. All rights reserved.

*Lecturer, Institute of Fluid Science.

$$\hat{U} = J\begin{bmatrix}\rho_1\\ \rho_2\\ \vdots\\ \rho_n\\ \rho u\\ \rho v\\ \rho w\\ E\end{bmatrix}, \qquad \hat{E} = J\begin{bmatrix}\rho_1 U\\ \rho_2 U\\ \vdots\\ \rho_n U\\ \rho u U + \xi_x p\\ \rho v U + \xi_y p\\ \rho w U + \xi_z p\\ (E+p)U\end{bmatrix}$$

$$\hat{E}_v = \frac{J}{Re_0}\begin{bmatrix}-\rho_1 v_{1i}\dfrac{\partial \xi}{\partial x_i}\\ -\rho_2 v_{2i}\dfrac{\partial \xi}{\partial x_i}\\ \vdots\\ -\rho_n v_{ni}\dfrac{\partial \xi}{\partial x_i}\\ \dfrac{\partial \xi}{\partial x_i}\tau_{1i}\\ \dfrac{\partial \xi}{\partial x_i}\tau_{2i}\\ \dfrac{\partial \xi}{\partial x_i}\tau_{3i}\\ \dfrac{\partial \xi}{\partial x_i}(u_j\tau_{ij} - q_i)\end{bmatrix}, \qquad \hat{S} = \frac{J}{D_{a0}}\begin{bmatrix}\dot{\omega}_1\\ \dot{\omega}_2\\ \vdots\\ \dot{\omega}_n\\ 0\\ 0\\ 0\\ 0\end{bmatrix} \tag{2}$$

As just shown, instead of solving the total density and $n-1$ species equation, the present scheme solves n species equations in a fully coupled fashion. Therefore, the concentrated computation error on the nth species can be avoided. In preceding equations, J is the Jacobian of coordinate transformation; Re_0 and D_{a0} are, respectively, the Reynolds number and Damköhler number based on the reference parameters; and U is the contravariant velocity in ξ direction

$$U = \xi_x u + \xi_y v + \xi_z w \tag{3}$$

The quantities t, u, v, and w are, respectively, time and the Cartesian velocities; ρ is the total density; ρ_i and f_i are the density and mass fraction of species i; and p is the sum of the partial pressures of each species. By assuming that the ideal gas equation is applicable to all of the species, the state equation becomes

$$p = \sum_{j=1}^{n} \rho_j R_j T \tag{4}$$

where R_j is the gas constant of species j, and T is the temperature. In terms of p, the total energy E can be written as

$$E = \sum_{j=1}^{n} \rho h_j f_j - p + \frac{\rho}{2}(u^2 + v^2 + w^2) \tag{5}$$

where enthalpy h_j is

$$h_j = h_{fj}^0 + \int_{T_{\text{ref}}}^{T} C_{pj}\,dT \tag{6}$$

where T_{ref} is the reference temperature, and h_{fj}^0 is the heat of formation of species j. The specific heat C_{pj} for each species is computed by a fourth-order polynomial of temperature that fits the data tabulated in JANAF.

The terms τ_{ij}, q_j, and v_{ij} are the shear stress tensor, heat flux, and diffusion velocity, respectively. By making the Stokes assumption for bulk viscosity, Fourier heat law for heat conduction, and Fick's law for molecular diffusion, τ_{ij}, q_j, and v_{ij} can be written as

$$\begin{aligned}\tau_{ij} &= -\mu\left(\frac{\partial u_i}{\partial x_j} + \frac{\partial u_j}{\partial x_i}\right) - \lambda\frac{\partial u_k}{\partial x_k}\delta_{ij}, \qquad \lambda = -\frac{2}{3}\mu\\ q_j &= -k\frac{\partial T}{\partial x_j} + \rho\sum_{j=1}^{n} f_i h_i v_{ij}\\ \rho_i v_{ij} &= -\rho D_i\frac{\partial f_i}{\partial x_j}\end{aligned} \tag{7}$$

where the viscosity μ, thermal conductivity k, and diffusion coefficient D_i can be calculated from Hirschfelder's formula and Wilke's average.

High-Resolution Shock-Capturing Scheme

Consider the scaler hyperbolic conservation law

$$\frac{\partial u}{\partial t} + \frac{\partial f(u)}{\partial x} = 0 \tag{8}$$

where $a(u) = \partial f/\partial u$ is the characteristic speed. A general three point explicit difference scheme in conservation form can be written as

$$u_j^{n+1} = u_j^n - \lambda\left(f_{j+\frac{1}{2}}^n - f_{j-\frac{1}{2}}^n\right) \tag{9}$$

where $\lambda = \Delta t/\Delta x$ and $f_{j+1/2}^n$ is a numerical flux function. By applying the MUSCL approach to the preceding numerical flux to obtain a higher order difference scheme, $f_{j+1/2}^n$ can be written as

$$\begin{aligned}f_{j+\frac{1}{2}} = \big[f\big(u_{j+\frac{1}{2}}^L\big) + f\big(u_{j+\frac{1}{2}}^R\big) - \big|a\big(u_{j+\frac{1}{2}}^L, u_{j+\frac{1}{2}}^R\big)\big|\\ \times\big(u_{j+\frac{1}{2}}^R - u_{j+\frac{1}{2}}^L\big)\big]/2\end{aligned}$$

with

$$\begin{aligned}u_{j+\frac{1}{2}}^R &= u_{j+1} - \frac{1-\phi}{4}\Delta u_{j+1}^R - \frac{1+\phi}{4}\Delta u_{j+1}^L\\ u_{j+\frac{1}{2}}^L &= u_j + \frac{1-\phi}{4}\Delta u_j^L + \frac{1+\phi}{4}\Delta u_j^R\end{aligned} \tag{10}$$

To eliminate the unwanted oscillations at the contact interface like shocks, various limiters are employed in evaluating $\Delta u_j^{R,L}$. A popular one is to use the minmod limiter to modify the upwind-biased interpolation as

$$\begin{aligned}\Delta u_j^R &= \text{minmod}\left(\Delta u_{j+\frac{1}{2}},\ \omega\Delta u_{j-\frac{1}{2}}\right)\\ \Delta u_j^L &= \text{minmod}\left(\Delta u_{j-\frac{1}{2}},\ \omega\Delta u_{j+\frac{1}{2}}\right)\end{aligned} \tag{11}$$

where

$$\text{minmod}(x, \omega y) = \text{Sign}(x)\text{Max}\{0, \text{Min}[|x|,\ \omega y\,\text{Sign}(x)]\}$$

$$\Delta u_{j+\frac{1}{2}} = u_{j+1} - u_j$$

and $1 \le \omega \le (3-\phi)/(1-\phi)$ for $\phi \ne 1$.

The spatial order of the accuracy of the preceding scheme is at most third order when ϕ takes the value 1/3. To capture the complex flow pattern beside shocks, a higher order scheme is needed. This can be realized directly by adding higher order terms to the third-order scheme (ϕ=1/3). Rewriting $u_{j+1/2}^{R,L}$ in the form as[4]

$$\begin{aligned}u_{j+\frac{1}{2}}^R &= u_{j+1} - \tfrac{1}{6}\bar{\Delta}u_{j+1}^R - \tfrac{1}{3}\bar{\Delta}u_{j+1}^L\\ u_{j+\frac{1}{2}}^L &= u_j + \tfrac{1}{6}\bar{\Delta}u_j^L + \tfrac{1}{3}\bar{\Delta}u_j^R\end{aligned} \tag{12}$$

with

$$\begin{aligned}\bar{\Delta}u_j^R &= \text{minmod}\big(\bar{\Delta}u_{j+\frac{1}{2}},\ \omega\bar{\Delta}u_{j-\frac{1}{2}}\big)\\ \bar{\Delta}u_j^L &= \text{minmod}\big(\bar{\Delta}u_{j-\frac{1}{2}},\ \omega\bar{\Delta}u_{j+\frac{1}{2}}\big)\\ \bar{\Delta}u_{j+\frac{1}{2}} &= \Delta u_{j+\frac{1}{2}} - \bar{\Delta}^3 u_{j+\frac{1}{2}}/6\end{aligned}$$

It can be seen that the preceding scheme is the same as the third-order MUSCL scheme except for the higher order term

$$\bar{\Delta}^3 u_{j+\frac{1}{2}} = \Delta^\alpha u_{j-\frac{1}{2}} - 2\Delta^\beta u_{j+\frac{1}{2}} + \Delta^\gamma u_{j+\frac{3}{2}} \tag{13}$$

where

$$\begin{aligned}\bar{\Delta}^\alpha u_{j-\frac{1}{2}} &= \text{minmod}\big(\Delta_{j-\frac{1}{2}},\ \sigma\Delta u_{j+\frac{1}{2}},\ \sigma\Delta u_{j+\frac{3}{2}}\big)\\ \bar{\Delta}^\beta u_{j+\frac{1}{2}} &= \text{minmod}\big(\Delta_{j+\frac{1}{2}},\ \sigma\Delta u_{j-\frac{1}{2}},\ \sigma\Delta u_{j+\frac{3}{2}}\big)\\ \bar{\Delta}^\gamma u_{j+\frac{3}{2}} &= \text{minmod}\big(\Delta_{j+\frac{3}{2}},\ \sigma\Delta u_{j-\frac{1}{2}},\ \sigma\Delta u_{j+\frac{1}{2}}\big)\end{aligned}$$

and σ is about 2.

The preceding scheme is a fourth-order TVD scheme. It has an advantage that the higher order term can be directly added to the third-order scheme with only little increase of CPU time.

Extension to Nonlinear System

Applying the scalar numerical flux to a nonlinear system defined in Eq. (10), we can obtain a new numerical flux

$$\hat{E}_{j+\frac{1}{2}} = \left[\hat{E}\left(\hat{U}^R_{j+\frac{1}{2}}\right) + \hat{E}\left(\hat{U}^L_{j+\frac{1}{2}}\right) - \left|A\left(\hat{U}^R_{j+\frac{1}{2}}, \hat{U}^L_{j+\frac{1}{2}}\right)\right|\left(\hat{U}^R_{j+\frac{1}{2}} - \hat{U}^L_{j+\frac{1}{2}}\right)\right]/2 \tag{14}$$

where

$$\left|A\left(\hat{U}^R_{j+\frac{1}{2}}, \hat{U}^L_{j+\frac{1}{2}}\right)\right| = \left[R_{j+\frac{1}{2}}|\Lambda|R^{-1}_{j+\frac{1}{2}}\right]^{R,L}$$

$$|\Lambda| = \mathrm{Diag}\left[|\lambda_1|, |\lambda_2|, \ldots, |\lambda_{n+4}|\right]$$

means the average Jacobian matrix of $A = \partial\hat{E}/\hat{U}$ defined by $\hat{U}^R_{j+1/2}$ and $\hat{U}^L_{j+1/2}$. The terms R and R^{-1} are the matrices consisting of the right and left eigenvectors of A with eigenvalues

$$\begin{aligned} \lambda_i &= U, \qquad i = 1, n+2 \\ \lambda_{n+3} &= U + c\sqrt{\xi_x^2 + \xi_y^2 + \xi_z^2} \\ \lambda_{n+4} &= U - c\sqrt{\xi_x^2 + \xi_y^2 + \xi_z^2} \end{aligned} \tag{15}$$

with

$$c^2 = \sum_{j=1}^{n} f_j \frac{\partial p}{\partial \rho_j} + \frac{\partial p}{\partial E}[(E+p)/\rho - (u^2 + v^2 + w^2)]$$

By using Beam–Warming splitting techniques, the linearized vector of $|A|\hat{U}^{R,L}$ in Eq. (14) can be written as

$$\begin{aligned} &\left|A\left(\hat{U}^R_{j+\frac{1}{2}}, \hat{U}^L_{j+\frac{1}{2}}\right)\right|\hat{U}^S = \hat{U}^S|\lambda_1| \\ &+ \frac{J}{c}\begin{pmatrix} f_1\rho^S\Delta U^S \\ \vdots \\ f_n\rho^S\Delta U^S \\ \rho^S u\Delta U^S + \tilde{\xi}_x\bar{P}^S \\ \rho^S v\Delta U^S + \tilde{\xi}_y\bar{P}^S \\ \rho^S w\Delta U^S + \tilde{\xi}_z\bar{P}^S \\ \rho^S H\Delta U^S + U_{\tilde{\xi}}\bar{P}^S \end{pmatrix}|\lambda_\alpha| \\ &+ \frac{J}{c^2}\begin{pmatrix} f_1\bar{P}^S \\ \vdots \\ f_n\bar{P}^S \\ \tilde{\xi}_x c^2\rho^S\Delta U^S + u\bar{P}^S \\ \tilde{\xi}_y c^2\rho^S\Delta U^S + v\bar{P}^S \\ \tilde{\xi}_z c^2\rho^S\Delta U^S + w\bar{P}^S \\ U_{\tilde{\xi}} c^2\rho^S\Delta U^S + H\bar{P}^S \end{pmatrix}|\lambda_\beta| \end{aligned} \tag{16}$$

where

$$\begin{aligned} \tilde{\xi}_i &= \xi_i/\sqrt{\xi_x^2 + \xi_y^2 + \xi_z^2}, \qquad U_{\tilde{\xi}} = U/\sqrt{\xi_x^2 + \xi_y^2 + \xi_z^2} \\ |\lambda_\alpha| &= (|\lambda_{n+3}| - |\lambda_{n+4}|)/2 \\ |\lambda_\beta| &= -|\lambda_1| + (|\lambda_{n+3}| + |\lambda_{n+4}|)/2 \\ \bar{P}^S &= \sum_{j=1}^{n}\frac{\partial p}{\partial \rho_j}\rho_j^S + \frac{\partial p}{\partial E}\left(E^S - \rho^S\sum_{j=1}^{n}u_j u_j^S\right) \\ \Delta U^S &= \tilde{\xi}_x(u^S - u) + \tilde{\xi}_y(v^S - v) + \tilde{\xi}_z(w^S - w) \end{aligned} \tag{17}$$

where S represents R and L. The variables with superscript S are computed from $\hat{U}^R_{j+1/2}$ or $\hat{U}^L_{j+1/2}$, and other variables should be computed from the generalized Roe-type average.

Time-Accurate LU-SGS Scheme

The LU scheme was originally developed by Jameson and Yoon.[15] This scheme has much higher computation efficiency and stability than the alternating direction implicit scheme, especially for multidimensional poblem. By splitting

$$\begin{aligned} A^\pm &= (A \pm r_A I)/2, \qquad B^\pm = (B \pm r_B I)/2 \\ C^\pm &= (C \pm r_C I)/2 \end{aligned} \tag{18}$$

where $r_A \geq \max|\lambda_A|$, $r_B \geq \max|\lambda_B|$, and $r_C \geq \max|\lambda_C|$; I is the unit matrix; and A, B, and C are the Jacobians of $\hat{E}$, $\hat{F}$, and $\hat{G}$, respectively.

The first-order implicit upwind difference scheme of Eq. (1) can be written as

$$\begin{aligned} &(I - \theta\Delta t H)[I + \theta\Delta t(\nabla_\xi A^+ + \nabla_\eta B^+ + \nabla_\zeta C^+ \\ &\quad + \Delta_\xi A^- + \Delta_\eta B^- + \Delta_\zeta C^-)]\Delta\hat{U}^n = RHS^n \end{aligned}$$

where

$$\begin{aligned} RHS^n &= -\Delta t\left(\frac{\partial\hat{E}}{\partial\xi} + \frac{\partial\hat{F}}{\partial\eta} + \frac{\partial\hat{G}}{\partial\zeta}\right)^n \\ &\quad + \Delta t\left(\frac{\partial\hat{E}_v}{\partial\xi} + \frac{\partial\hat{F}_v}{\partial\eta} + \frac{\partial\hat{G}_v}{\partial\zeta} + \hat{S}\right)^n \end{aligned} \tag{19}$$

where H is the Jacobian matrix of source term, $H = \partial\hat{S}/\partial\hat{U}$, and ∇ and Δ are backward and forward difference operators. The higher order TVD solver, which was given in Eq. (12), is used to calculate the convection term of RHS^n.

With the definition of $A^\pm$, $B^\pm$, and $C^\pm$, a first-order LU-SGS scheme can be written as

$$\begin{aligned} &(I - \theta\Delta t H)[I + \theta\Delta t(\nabla_\xi A^+ + \nabla_\eta B^+ + \nabla_\zeta C^+ \\ &\quad - A^- - B^- - C^-)][I + \theta\Delta t(A^+ + B^+ + C^+ - A^- \\ &\quad - B^- - C^-)]^{-1}[I + \theta\Delta t(\Delta_\xi A^- + \Delta_\eta B^- + \Delta_\zeta C^- \\ &\quad + A^+ + B^+ + C^+)]\Delta\hat{U}^n = RHS^n \end{aligned} \tag{20}$$

or

$$\begin{aligned} &[I - \theta\Delta t H + \theta\Delta t(\nabla_\xi A^+ + \nabla_\eta B^+ + \nabla_\zeta C^+ \\ &\quad - A^- - B^- - C^-)][I - \theta\Delta t H + \theta\Delta t(A^+ + B^+ + C^+ \\ &\quad - A^- - B^- - C^-)]^{-1}[I - \theta\Delta t H + \theta\Delta t(\Delta_\xi A^- + \Delta_\eta B^- \\ &\quad + \Delta_\zeta C^- + A^+ + B^+ + C^+)]\Delta\hat{U}^n = RHS^n \end{aligned} \tag{21}$$

where θ is a parameter. If $\theta = 1$, the preceding scheme becomes fully implicit.

As shown earlier, the fourth-order TVD scheme has been combined with the LU-SGS method. However, its time accuracy is only first order, which is not accurate enough to simulate a time-dependent problem with a large CFL number. A time accurate scheme can be obtained by employing the Crank–Nicholson method. Equations (20) and (21) can be rewritten in the form

$$L^m\Delta\hat{U}^m = RHS^m \tag{22}$$

with

$$\begin{aligned} \Delta\hat{U}^m &= \hat{U}^{m+1} - \hat{U}^m \\ RHS^m &= -(\hat{U}^m - \hat{U}^n) + [RHS(\hat{U}^m) + RHS(\hat{U}^n)]/2 \end{aligned}$$

where L represents the left difference operators in Eqs. (20) and (21); n and m are, respectively, the number of time steps and the number of Newton iterations. Therefore, $\hat{U}^{m+1} = \hat{U}^m + \Delta\hat{U}^m$ is the mth approximation of $\hat{U}^{n+1}$. With this algorithm, a converged time-accurate solution of $\hat{U}^{n+1}$ can be obtained within a few iterations.

Diagonal Algorithm and Local Implicit Technique

There are many combustion problems in which only a steady-state solution is desired and the time-dependent equations are used merely as a tool for the iteration solution of steady state. Since the existing point-implicit scheme needs the inversion of the Jacobian matrix at each grid point and thus is very expensive for simulating the problems with finite rate chemistry, an efficient diagonal algorithm is greatly needed. Generally, the left implicit operator in Eq. (22) does not affect the steady-state solution because the residual term RHS finally goes to zero. However, since the finite rate chemistry is strongly nonlinear, an improper simplification of the implicit operator will result in a nonphysical solution. For example, it is well known that numerical simulation of flames in a mixing layer or in a counter flow always leads to two converged solutions,[16,17] physical and nonphysical solutions. Therefore, to obtain a reasonable diagonal algorithm, attention should be paid to the kinetics of chemical reaction.

For supersonic combustion, ignition and flame holding of hydrogen/air is a specially attractive object of our interest, because it is of special relevance to the propulsion system of supersonic vehicles and its detailed kinetic mechanism has been made clear. In the hydrogen/air system, reaction is initiated from $H_2 + O_2 \rightarrow H + HO_2$ (I). This procession triggers the chain branching reactions $O_2 + H \rightarrow OH + O$ (II), $H_2 + O \rightarrow OH + H$ (III), and $H_2 + OH \rightarrow H_2O + H$ (IV). With the increase of the concentration of H, $H + O_2 + M \rightarrow HO_2 + M$ (V) then comes into stage to compete with reaction I and to produce HO_2 with a large heat release. The produced HO_2 is consequently consumed through $HO_2 + H \rightarrow 2OH$ (VI) and $HO_2 + H \rightarrow H_2O + O$ (VII). Although there are a lot of other reactions, recent studies of kinetics[18,19] have shown that the preceding elementary reactions dominate the whole process of ignition and flame holding. Therefore, production and consumption of a certain species are, respectively, controlled by these elementary reactions. For example, O is mainly produced via I and consumed via III, and HO_2 is mainly produced via V and consumed via VI and VII. Thus, for simulating the finite rate phenomena, the individual characteristic time of the elementary reactions, not the sum of them, should be taken into account.

By writing the backward reactions in the form of forward reactions, the mass reaction rate of species j can be written as

$$\dot{\omega}_j = M_j \sum_{i=1}^{NR} \left(\sum_{k=1}^{n} \alpha_{ki} C_k \right)^{\beta_i} (\gamma''_{ij} - \gamma'_{ij}) \times A_i T^{N_i} \exp^{-E_i/R_0 T} \prod_{k=1}^{n} C_k^{\gamma'_{ik}} \tag{23}$$

where NR is the total reaction number and α_{ki} is the third body efficiency. To consider the individual characteristic time of production and consumption, $\dot{\omega}_j$ can be rewritten in the form

$$\dot{\omega}_j = \dot{\omega}_j^p - \dot{\omega}_j^c \tag{24}$$

where $\dot{\omega}_j^p$ and $\dot{\omega}_j^c$, respectively, represent the production term and consumption term in Eq. (23).

For constructing a diagonal scheme, the implicit reaction solver in Eq. (20) can be written as[13]

$$(I - \theta \Delta t H) \Delta \hat{U}^n = [I + \theta \mathrm{Diag}(\Delta t / \tau_j)] \Delta \hat{U}^n = RHS^n \tag{25}$$

where τ_j is the characteristic time of production or consumption of species j. The problem is how to define a τ_j that represents the physical characteristic time of the elementary reaction. Eberhart and Imlay used the two-norm of row j of matrix H as the definition of τ_j. Although this definition eliminated the stiffness of the source term, it does not reflect the kinetics of elementary reaction.

Based on the preceding analysis of the reaction kinetics of hydrogen/air, in the present study, we define τ_j as

$$\tau_j^{-1} = \mathrm{Max}\left[\frac{\partial \dot{\omega}_j^c}{\partial \rho_j}, \left. \frac{\partial \dot{\omega}_j^p}{\partial \rho_k} \right|_{k \neq j} \right] \tag{26}$$

The first term on the right-hand side of the preceding equation represents the inverse of consumption characteristic time of elementary reactions in which species j is the reactant. The second term represents the inverse of production characteristic time of the elementary reaction in which species j is the product ($\partial \dot{\omega}_j^p / \partial \rho_k$ is neglected here because the characteristic time of reaction i is included in $\partial \dot{\omega}_j^c / \partial \rho_j$). Therefore, whether the species is dominated by consumption or production depends only on the elementary reaction itself, not the sum of them.

In addition, there are many other combustion problems in which a time-accurate solution is desired. Therefore, inversion of the full Jacobian matrix is inevitable, although it is very time consuming. As mentioned earlier, many existing schemes[10-13] do this inversion at each grid point.

An independent fact is that flame thickness is only of the order of 0.1 mm. This phenomenon motivated the idea of asymptotic analysis,[16,17] in which the analytical region is always divided into two parts, the reaction zone and the reaction frozen zone. In the wide reaction frozen zone, chemical reactions are neglected. Only the reactions being confined to the very narrow reaction zone are considered. This method greatly simplifies the complexity of the analysis and has significantly enhanced our understanding of the combustion phenomena.

In the high-speed combustion problem, ignition and combustion are dominated by the diffusion mechanism. The reaction zone is very thin compared with the whole physical domain. Thus, the stiffness problem caused by the fast proceeding of chemical reactions is only confined to this very thin reaction zone. Therefore, it is worthwhile to use the idea of the asymptotic analysis in our numerical simulation; that is, it is only necessary to treat the stiffness in the very narrow reaction zone. In the wide outer region, since the chemical reactions are almost frozen, the reaction source term can be treated explicitly. This local implicit method will dramatically save the computational time because the matrix inversion is not needed at the initial slow reaction stage and is only needed at the grid points in the thin reaction zone. Furthermore, this method preserves time accuracy.

The problem is how to determine the location of the reaction zone. In the present study, we use the following expression:

$$\mathrm{Max}[\dot{\omega}_1, \dot{\omega}_2, \ldots, \dot{\omega}_n] \geq \dot{\omega}_0 \tag{27}$$

as an approximate evaluation. In the present simulation, $\dot{\omega}_0$ is set to 1. A larger $\dot{\omega}_0$ is also acceptable, but the computation efficiency is not linearly dependent on the choice.

Numerical Results

An unsteady two-dimensional, nonreacting, supersonic flow in a ramped duct is first chosen to show the validity of the present numerical algorithm. Since the same flow has been computed by a number of CFD research groups,[4] the resolution of the present scheme can be easily understood through the comparison. The geometry and inflow conditions of the test case are illustrated in Fig. 1. The computation grid used here has 241 × 81 grid points, the CFL number is 10, and m in Eq. (22) is set to 2 for the time accuracy. Figure 2 is a comparison of an instantaneous contour of Mach number at a typical nondimensional time ($t = 5.0$), respectively, calculated by using the first-order upwind Roe scheme, the second-order Harten–Yee TVD scheme, the third-order MUSCL TVD scheme, and the present scheme with the same computational program. To show the original characteristics of stability and accuracy of these schemes, no artificial dissipations are added in the calculations. It can be seen that the first-order Roe scheme cannot even give out the shock near the exit of the duct due to its large numerical viscosity. Although the

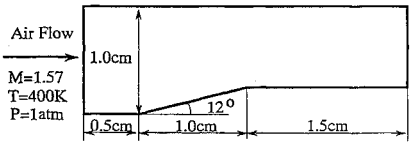

Fig. 1 Geometry and inflow conditions of an unsteady supersonic duct flow.

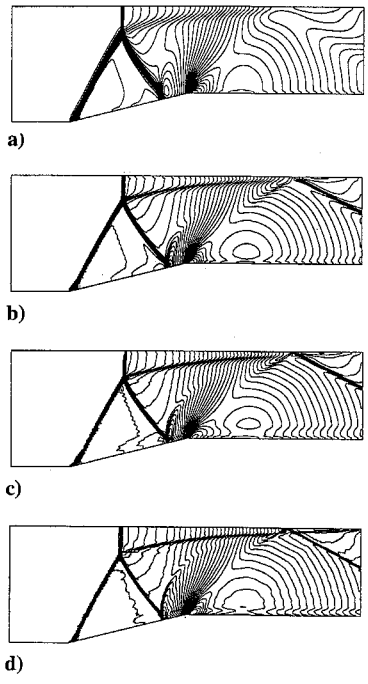

Fig. 2 Comparison of an instantaneous contour of Mach number at a typical nondimensional time ($t = 5.0$) with different numerical schemes. a) first-order upwind Roe scheme, b) second-order Harten–Yee TVD scheme, c) third-order MUSCL TVD scheme, and d) the present scheme.

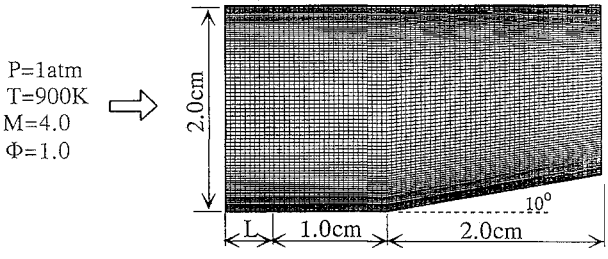

Fig. 3 Geometry and inflow conditions for the premixed H_2/ air reacting flow in a ramped duct.

second-order Harten–Yee TVD scheme and the third-order MUSCL scheme greatly improved their accuracies, the present scheme gives out much sharper and clearer resolution of shocks and slip line than the other three. Furthermore, only the present scheme can clearly show the pattern of shock reflection at the upper wall of duct.

The next case considered for code assessment is the combustion of a premixed hydrogen/air supersonic flow in a ramped duct. The same flows also have been computed by a number of CFD groups.[10,11,20] The geometry and inflow conditions are illustrated in Fig. 3. The duct is 3 cm long and 2 cm high. To avoid the abrupt change of flow velocity at the boundary layers of the flow entrance, an inviscid duct with the length of L is added before the testing duct. The finite rate chemistry[19] that includes 9 species and 33 elementary reactions is employed. The pressure graph with 78 × 101 grid points is shown in Fig. 4. It can be seen that the initial inviscid duct being added does not cause any changes of pressure. However, at the entrance of viscous duct, two leading-edge shocks caused by the upper and lower boundary layers are clearly seen. The normalized pressure, temperature, and mass fraction of species at the ramp of the bottom wall are shown in Fig. 5. The results are calculated along the y station located 0.13 cm from the bottom wall. It can be seen that the agreement is reasonably good. The present results show a little longer ignition delay time and narrower reaction zone than that of Uenishi. This may be attributed to the difference of chemical model.

Another purpose of the present study is to show the applicability of the diagonal algorithm and local implicit method to finite

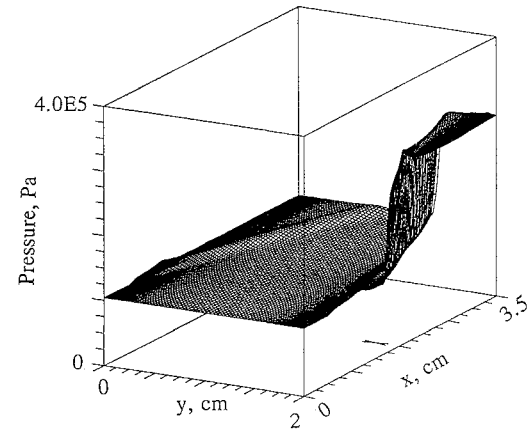

Fig. 4 Distribution of static pressure.

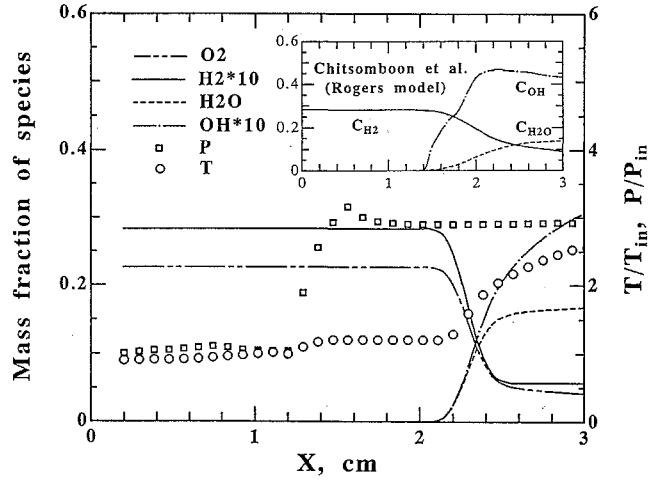

Fig. 5 Profiles of normalized species mass fractions, pressure, and temperature along $y = 0.13$ cm.

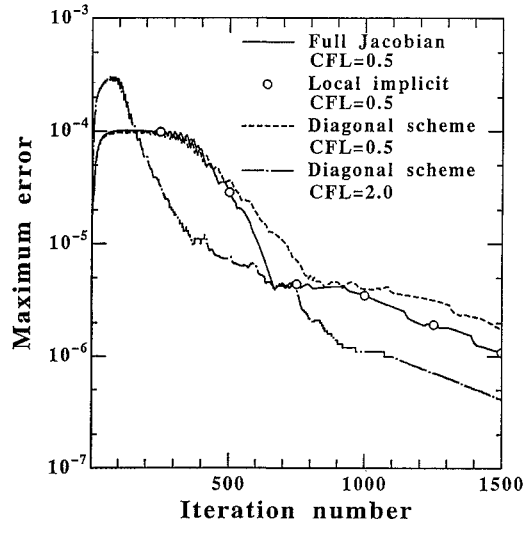

Fig. 6 Comparison of histories of maximum residuals of $\Delta\hat{U}$.

rate chemistry by comparing them with the full Jacobian implicit method. In the diagonal algorithm, the Jacobian H of reaction source term is diagonalized by using Eqs. (25) and (26). In the full Jacobian implicit method, the Jacobian H is inverted at every grid point of the computation domain. In the local implicit method, the Jacobian H is only inverted at the grid points within the reaction zone, which is determined through Eq. (27). Here, the shock-induced ignition problem discussed earlier is chosen as an objective of this comparison. The history of maximum residual of $\Delta\hat{U}$ calculated from these three methods is shown in Fig. 6. It can be seen that for $\hat{\omega}_0 = 1$

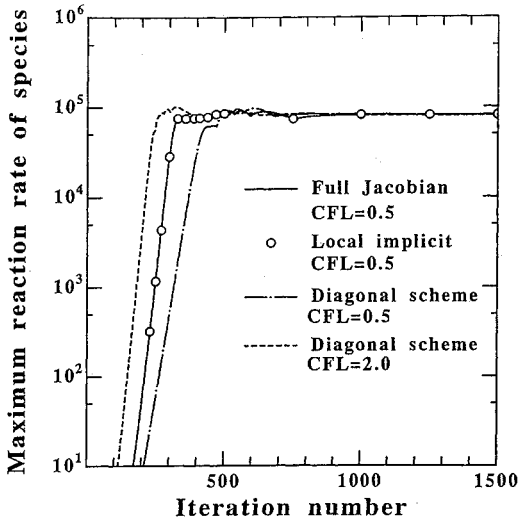

Fig. 7 Comparison of histories of maximum reaction rates.

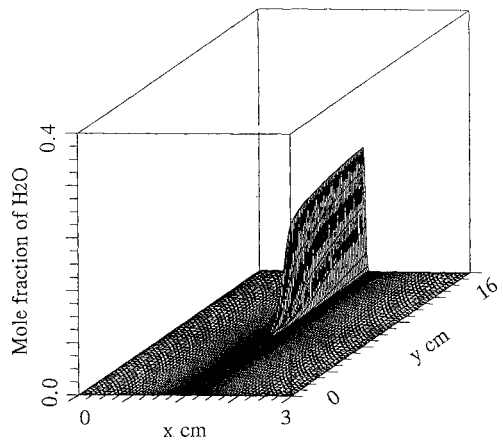

Fig. 8 Illustration of ignition of nonpremixed H_2/air or CH_4/air streams in a supersonic mixing layer.

the local implicit method gives the same results as that of the full Jacobian method. However, the local implicit method saves about 30% of the total computation time. This improvement is significant. The diagonal scheme is much more efficient; it reduces the total CPU time to only 40%. Furthermore, the convergence rate of diagonal form is nearly the same as that of the full Jacobian method. It can also be seen that, by raising the CFL number from 0.5 to 2.0, convergence rate is greatly accelerated.

In Fig. 7, the corresponding histories of the maximum reaction rate of species ($\dot{\omega}_{H_2O}$) calculated from these methods are illustrated. The results show that all of these methods converge to the same steady-state solution after 1000 iterations. The use of the diagonal scheme delays the initial proceeding of the reactions because it uses the minimum characteristic time of the elementary reactions as the characteristic time of production or consumption of a certain species. However, the local implicit method also gives the same results as the full Jacobian. Therefore, the local implicit method can be used for the time-accurate solution. Additionally, it can be seen that a moderate CFL number is efficient for steady-state simulation.

It has become clear that reaction kinetics of nonpremixed hydrogen/air system is more complex that its premixed system.[19] For confidence, the present method is also used for the ignition of two parallel nonpremixed hydrogen/air streams in a supersonic mixing layer. As can be seen in Fig. 8 (90 × 120 grid points), hydrogen, which was diluted by 40% of nitrogen, and air mix at the trailing edge of a smooth splitter and result in an ignition downstream. The two streams have equal temperatures, 1200 K, and equal pressures, 1 atm. The results calculated by the diagonal scheme and the local implicit method are, respectively, shown in Figs. 9 and 10. Comparison

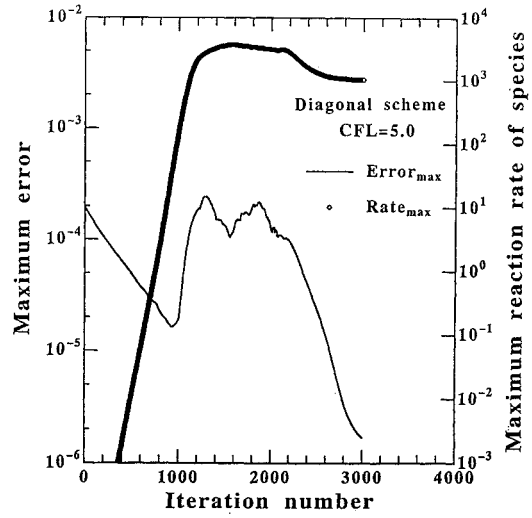

Fig. 9 Histories of maximum residuals and reaction rate of diagonal algorithm.

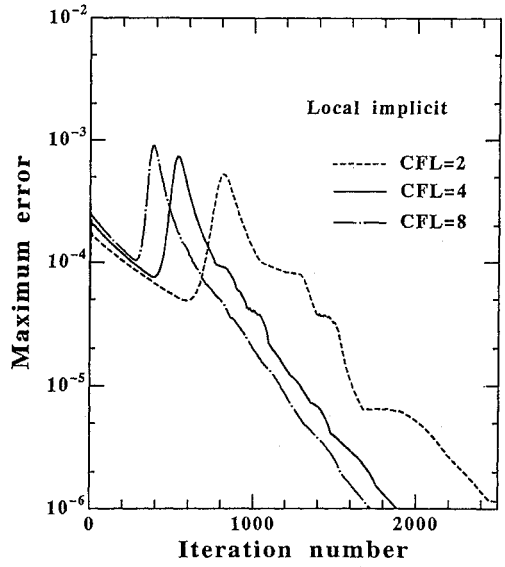

a)

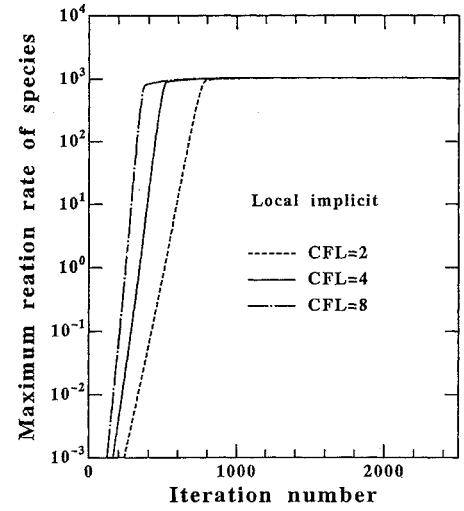

b)

Fig. 10 Histories of a) maximum residuals of local implicit algorithm and b) maximum reaction rates of local implicit algorithm.

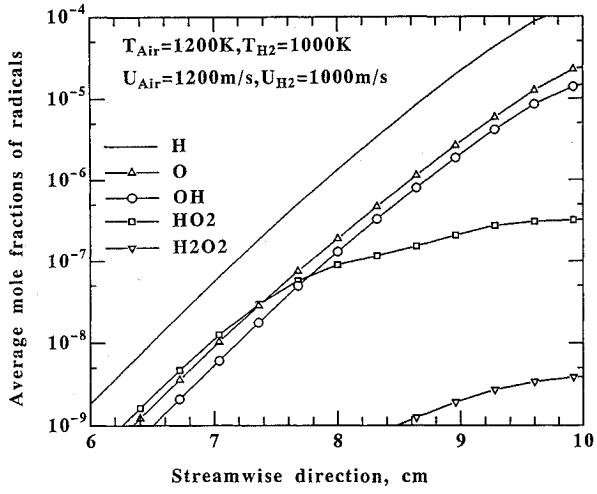

Fig. 11 Production rate of radicals along streamwise direction of nonpremixed H_2/air ignition in supersonic mixing layer.

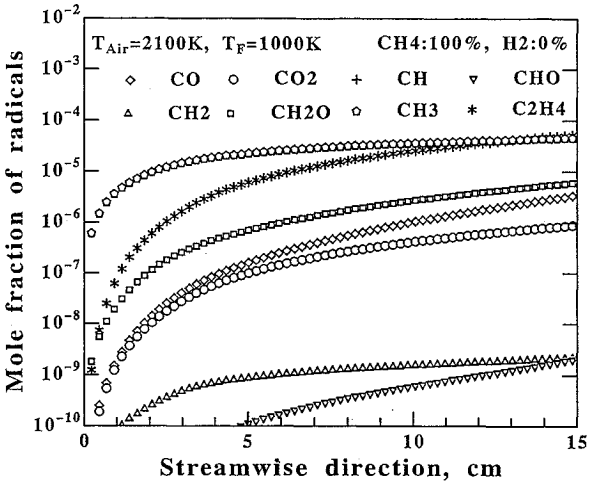

Fig. 12 Production rate of radicals along streamwise direction of nonpremixed CH_4/air ignition in supersonic mixing layer.

of these two figures indicates that the two schemes also converge to the same steady-state solution. Because of the existence of mixing process of fuel and air, the diagonal scheme requires 3000 iterations to achieve steady-state solution, whereas the local implicit scheme needs only 2000 iterations. Additionally, an increase of CFL number from 2 to 4 dramatically accelerated the convergence. Although further increase of CFL number is tried, choice of a CFL number between 1 to 20 is efficient. A too large CFL number may result in a nonphysical solution for finite rate problems.

Figure 11 shows the production rates of radicals along the streamwise direction. It can be seen that H and HO_2 are initially produced through reaction $H_2 + O_2 \rightarrow H + HO_2$. The production and consumption histories of other radicals are clearly captured. These results show that the present scheme is robust to study the kinetic chemistry of reaction.

To consider a more complex chemistry, the present scheme is finally used to calculate the ignition of a nonpremixed methane/air stream in a supersonic mixing layer (see Fig. 8). The finite rate chemistry includes 18 species and 101 elementary reactions.[21] The pressures of both streams are also set to 1 atm. Velocities of air stream and methane stream are, respectively, 1200 and 1000 m/s. Temperatures of air and methane streams are, respectively, 1000 and 2100 K. Production rates of radicals ($\int_0^H X_i\, dy$) before ignition along the streamwise direction are shown in Fig. 12. It is shown that CH_3 and C_2H_4 are, respectively, produced through $CH_4 \rightarrow H + CH_3$ and $CH_3 + CH_3 \rightarrow H_2 + C_2H_4$ and exist at high concentration before ignition. This phenomenon has been made clear by the study of Trevino and Mendez.[22] This agreement indicates that the present scheme is also effective to solve the complex reaction chemistry.

Conclusions

A high-resolution TVD scheme has been developed for calculating chemically reacting flows. Numerical test in an unsteady supersonic duct showed that the present scheme is superior to previous one. A diagonal implicit algorithm and a local implicit algorithm presented, respectively, for steady-state and time-accurate simulations of finite rate chemistry were tested by calculating ignitions of premixed and nonpremixed hydrogen/air systems. Comparison of the present algorithm with the point-implicit algorithm clearly showed that the present algorithm was efficient and robust. Furthermore, the use of the present algorithm to the ignition of nonpremixed methane/air streams in a supersonic mixing layer indicated that the present algorithm is capable of simulating complex chemistry. Combination of the present scheme with the LU-SGS scheme significantly improved the numerical efficiency and stability. In future efforts, interaction between turbulence and the finite rate chemistry should be considered.

Acknowledgments

The author would like to thank T. Niioka for his constant support in publishing this paper. The author also wishes to express his appreciation for many helpful discussions with Y. Wada and X. Yuan.

References

[1]Yee, H. C., Warming, R. F., and Harten, A., "Implicit Total Variation Diminishing (TVD) Schemes for Steady-State Calculations," *Journal of Computational Physics*, Vol. 57, 1985, pp. 327–360.

[2]Van Leer, B., "Towards the Ultimate Conservation Difference Scheme V, A Second-Order Sequel to Godunov's Method," *Journal of Computational Physics*, Vol. 32, 1979, pp. 101–136.

[3]Chakravarthy, S. R., and Osher, S., "High Resolution Applications of the Osher Upwind Schemes for the Euler Equations," AIAA Paper 83-1943, Jan. 1983.

[4]Yamamoto, S., and Daiguji, H., "High-Order Shock Capturing Schemes," *Reports of the Institute of Fluid Science* (Tohoku Univ.), Vol. 3, 1991, pp. 189–200.

[5]Wada, Y., Kubota, H., Ishiguro, T., and Ogawa, S., "A Fully Implicit High-Resolution Scheme for Chemically Reacting Compressible Flow," *Notes on Numerical Fluid Mechanics*, Vol. 24, Vieweg, Brunswick, Germany, 1988, pp. 648–659.

[6]Bird, G. A., "Direct Simulation of Typical AOTV Entry Flows," AIAA Paper 86-1310, Jan. 1986.

[7]Bussing, T. R. A., and Murman, E. M., "A Finite Volume Scheme for the Calculation of Compressible Chemically Reacting Flow," AIAA Paper 85-0331, Jan. 1985.

[8]Drummond, J. P., Rogers, R. C., and Hussaini, M. Y., "A Detailed Numerical Model of a Supersonic Reacting Mixing Layer," AIAA Paper 86-1427, June 1986.

[9]Candler, G. V., "The Computation of Weakly Ionized Hypersonic Flows in Thermochemical Nonequilibrium," Ph.D. Dissertation, Stanford Univ., Stanford, CA, June 1988.

[10]Yee, H. C., and Shinn, J. L., "Semi-Implicit and Fully Implicit Shock-Capturing Methods for Hyperbolic Conservation Laws with Stiff Source Terms," AIAA Paper 87-1116, June 1987.

[11]Shuen, J. S., and Yoon, S., "Numerical Study of Chemically Reacting Flows Using a Lower-Upper Symmetric Successive Overrelaxation Scheme," *AIAA Journal*, Vol. 27, No. 12, 1989, pp. 1752–1756.

[12]Yu, S., Tsai, Y. P., and Shuen, J. S., "Three-Dimensional Calculations of Supersonic Reacting Flows Using a LU Scheme," *Journal of Computational Physics*, Vol. 101, 1992, pp. 276–286.

[13]Eberhardt, S., and Imlay, S., "Diagonal Implicit Scheme for Computing Flows with Finite Rate Chemistry," *Journal of Thermophysics and Heat Transfer*, Vol. 6, 1992, pp. 208–215.

[14]Ju, Y., "Analytical and Numerical Study on Ignition and Combustion in a Supersonic Mixing Layer," Ph.D. Dissertation, Tohoku Univ., Sendai, Japan, March 1994.

[15]Jameson, A., and Yoon, S., "Lower-Upper Implicit Schemes with Multiple Grids for the Euler Equations," *AIAA Journal*, Vol. 25, No. 7, 1987, pp. 929–935.

[16]Liñán, A., "The Asymptotic Structure of Counterflow Diffusion Flames for Large Activation Energies," *Acta Astronatica*, Vol. 1, Pergamon, New York, 1974, pp. 1007–1039.

[17]Ju, Y., and Niioka, T., "Ignition Analysis of Unpremixed Reactants with Chain Mechanism in a Supersonic Mixing Layer," *AIAA Journal*, Vol. 31, No. 5, 1993, pp. 863–868.

[18]Trevino, C., *Ignition Phenomena in Hydrogen and Oxygen Mixtures*, Vol. 131, Progress in Astronautics and Aeronautics, AIAA, Washington, DC, 1990, p. 19.

[19]Ju, Y., and Niioka, T., "Reduced Kinetic Mechanism of Ignition for Non-Premixed Hydrogen/Air," *Combustion and Flame*, Vol. 99, 1994, pp. 240–246.

[20]Uenishi, R., Rogers, R. C., and Northam, G. B., "Three Dimensional Computations of Transverse Hydrogen Jet Combustion in a Supersonic Airstream," AIAA Paper 87-0089, June 1987.

[21]Stahl, G., and Warnatz, J., "Numerical Investigation of Time Dependent Properties and Extinction of Structure of Methane and Propane Air Flamelets," *Combustion and Flame*, Vol. 85, 1991, pp. 285–299.

[22]Trevino, C., and Mendez, F., "Reduced Kinetic Mechanism for Methane Ignition," *24th Symposium (International) on Combustion*, Combustion Inst., Pittsburgh, PA, 1992, pp. 121–127.